COMPARATIVE ANALYSES OF THE JANUARY 2004 COLD AIR OUTBREAK

A Thesis
Presented to
The Academic Faculty

by

Kelli Lynne Hornberger

In Partial Fulfillment
of the Requirements for the Degree
Master of Science in the
School of Earth and Atmospheric Sciences

Georgia Institute of Technology
August 2010

COMPARATIVE ANALYSES OF THE JANUARY 2004 COLD AIR OUTBREAK

Approved by:

Dr. Robert X. Black, Advisor
School of Earth and Atmospheric Sciences
Georgia Institute of Technology

Dr. Judith A. Curry
School of Earth and Atmospheric Sciences
Georgia Institute of Technology

Dr. Yi Deng
School of Earth and Atmospheric Sciences
Georgia Institute of Technology

Date Approved: May 21, 2010

To my family and friends for all their love and support throughout the pursuit of my education. To all my professors, teachers, and coaches who provided me with the knowledge and ability to follow my dreams.

ACKNOWLEDGEMENTS

The author would like to thank Dr. Robert X. Black for continued advisement and assistance throughout the research and writing process. Appreciation is extended to Brandon Miller in support of the project formulation and initiation. Finally, the author would like to recognize James Belanger and Jason Furtado for their continued assistance, comments, and suggestions on this work.

TABLE OF CONTENTS

LIST OF TABLES

Page

LIST OF FIGURES

Page

LIST OF ABBREVIATIONS

AO	Arctic Oscillation
ASOS	Automated Surface Observing System
CAO	cold air outbreak
EPV	Ertel potential vorticity
EWE	extreme weather event
HPC	Hydrometeorological Prediction Center
KABI	Abilene, Texas
KDDC	Dodge City, Kansas
KGSO	Greensboro, North Carolina
KGSP	Greer, South Carolina
KMEM	Memphis, Tennessee
MERRA	Modern Era Retrospective-Analysis for Research and Applications
NAO	North Atlantic Oscillation
NARR	North American Regional Reanalysis
NASA	National Aeronautic and Space Administration
NCAR	National Center for Atmospheric Research
NCEP	National Centers for Environmental Prediction
PNA	Pacific-North American pattern
PV	potential vorticity
PVU	potential vorticity unit
WCT	wind chill equivalent temperature

SUMMARY

Cold air outbreaks (CAOs) occur when large scale atmospheric circulations allow for the incursion of polar air masses into middle and lower latitudes, influencing wintertime temperatures regionally. The January 2004 CAO is identified as a major CAO in the Deep South of the United States in terms of wind chill equivalent temperature or a temperature-only criterion. Surface air temperature, horizontal winds, specific humidity, and Ertel potential vorticity are analyzed for this event using several reanalysis products: National Aeronautic and Space Administration Modern Era Retrospective-Analysis for Research and Application (MERRA), the National Centers for Environmental Prediction National Center for Atmospheric Research (NCEP-NCAR), and the National Centers for Environmental Prediction North American Regional Reanalysis (NARR). We perform an intercomparison of the reanalysis products and parallel surface station observations during the synoptic evolution of the leading cold front associated with CAO onset. The key synoptic, mesoscale, and dynamical features associated with onset are studied to determine the relative accuracy of the respective reanalysis products in representing the key features. The comparative evaluation revealed pronounced temperature and moisture biases in the NCEP-NCAR reanalysis products that limit its utility in portraying the synoptic features characteristic of CAO onset. Conversely, both MERRA and NARR accurately represent the detailed thermodynamic and moisture structural evolution associated with CAO onset indicating their utility in future observationally-based studies of CAO events. Ertel potential

vorticity analyses indicate that the onset of the 2004 CAO is strongly linked to an incipient tropopause fold feature that developed over the Great Lakes region.

CHAPTER 1

INTRODUCTION

Extreme weather events (EWEs) are weather phenomena with substantial impacts on society and the economy through energy consumption, agriculture loss, and risks to human health. EWEs include heat and cold waves, heavy precipitation events, tornadoes, and droughts. Heavily populated areas located within the United States at midlatitudes are strongly affected by these events. Cold air outbreaks (CAOs) are linked to regional impacts such as increased energy consumption, crop and livestock losses, disease, or even death. The citrus industry is particularly vulnerable to CAO events as shown by Rogers and Rohli (1991) and Downton and Miller (1993) who examined freeze risks associated with CAOs. The effect on human exposure can be devastating especially for the elderly, very young, mentally ill, and homeless people who are more susceptible when exposed to the cold. Between 1979 and 2002, an average of 689 deaths per year was attributed to exposure to excessive natural cold (O'Neill and Ebi 2009). It is clearly of societal importance to better understand the underlying physical nature of these events to improve their prediction and minimize their impact.

North American CAOs have been linked to large scale atmospheric circulations such as the Pacific-North American pattern (Rogers and Rohli 1991), the North Atlantic Oscillation (Downton and Miller 1993), and the Arctic Oscillation (Walsh et al. 2001), but little research has been conducted on the underlying dynamics, representation in general circulation models, or the medium-range predictability of these events. Previous studies have shown that CAOs are linked to variations in the polar vortex and various

teleconnection pattern indices (Cellitti et al. 2006), rapid surface cyclogenesis (Konrad and Colucci 1989), and diabatic and advective forcings (Portis et al. 2006). Recent statistical studies show no apparent trend in the frequency of future CAOs despite recent background warming trends (Walsh et al. 2001, Nogaj et al. 2006, Portis et al. 2006). The most recent findings reveal the importance of studying the regional characteristics of CAOs in any future changes that may occur.

Vavrus et al. (2006) defined a CAO as a surge of cold polar air into middle or lower latitudes that result in extreme negative anomalies of surface air temperature. Regionally, outbreaks that affect the East and Gulf coasts result from a detachment of cold air pools from high-latitude air masses while Midwestern outbreak events are more closely tied to continued cold air advection from air masses remaining in higher latitudes (Walsh et al. 2001). Traditional CAO definitions are based solely on temperature anomalies to classify and rank noteworthy events, but the influence of CAOs on energy consumption and human exposure is also a function of how quickly heat is transported away from a building or body. In order to fully quantify the impact of CAOs, other measures like wind chill indices, heating and cooling degree days, and power consumption need to be considered. In this study, the January 2004 CAO was identified as a major event over the Deep South from either a temperature only criterion or a wind chill equivalent temperature (WCT) approach (Osczevski and Bluestein 2005). The WCT incorporates wind and temperature:

$$WCT=13.12+0.6215T-11.37V^{0.16}+0.3965TV^{0.16}$$

where air temperature is in °C and wind speed is in km h^{-1}. The motivation for the current study was to characterize the synoptic evolution of CAO onset, comparatively

asses the ability of various reanalysis datasets to represent key synoptic and mesoscale features associated in CAO onset, and provide initial dynamical characterization of primary potential vorticity features in CAO onset for the January 2004 event. As a major event that impacted the Deep South, the characterization of the event is important to guide future studies of CAO dynamics and prediction.

CHAPTER 2

DATA AND METHODOLOGY

The three main datasets used in characterizing the January 2004 cold air outbreak (CAO) were the National Aeronautic and Space Administration (NASA) Modern Era Retrospective-Analysis for Research and Applications (MERRA), the National Centers for Environmental Prediction National Center for Atmospheric Research (NCEP-NCAR, hereafter NCEP), and the National Centers for Environmental Prediction North American Regional Reanalysis (NCEP-NARR, hereafter NARR). MERRA has a horizontal spatial resolution of 1/2° latitude by 2/3° longitude for hourly two-dimensional time averaged fields and a spatial resolution of 1.25° latitude by 1.25° longitude on forty-two pressure levels for the three-hourly three-dimensional instantaneous fields (Suarez et al. 2008). The two-dimensional fields utilized in the study were two-meter and 850 hPa air temperatures, two-meter and 850 hPa wind fields, and two-meter specific humidity while Ertel potential vorticity was the only three-dimensional field used. The NCEP-NCAR 40-Year Reanalysis (Kalnay et al. 1996) contained fields on 4x-daily grids with horizontal resolutions of 2.5° latitude by 2.5° longitude. The fields used here were the surface air temperature (from the lowest model level, $\sigma = 0.995$) and the two-meter specific humidity. The NARR data employed, two-meter air temperature and specific humidity, are available every three hours at 32-km grid spacing (Mesinger et al. 2006).

The three datasets discussed above were evaluated and compared to Automated Surface Observing System (ASOS) hourly observations during the CAO of January 2004. The data provided from the station observations included the dry bulb temperature, dew

point temperature, wet bulb temperature, relative humidity, wind speed, station pressure, and sea level pressure, but only the dry bulb temperature, dew point temperature, and station pressure were exploited. ASOS stations were selected based on their latitude and longitude coordinates, to be colocated within twenty miles of a common grid point between MERRA and NCEP datasets. The following cities displayed in Figure 1 were selected based on their proximity to reanalysis grid points: Abilene (KABI), Dodge City (KDDC), Greensboro (KGSO), Greer (KGSP), Memphis (KMEM), and Roanoke (KROA). Both temperature and specific humidity analyses were extracted from reanalysis datasets and then compared to the ASOS stations to determine which reanalysis product best represent the CAO's evolution.

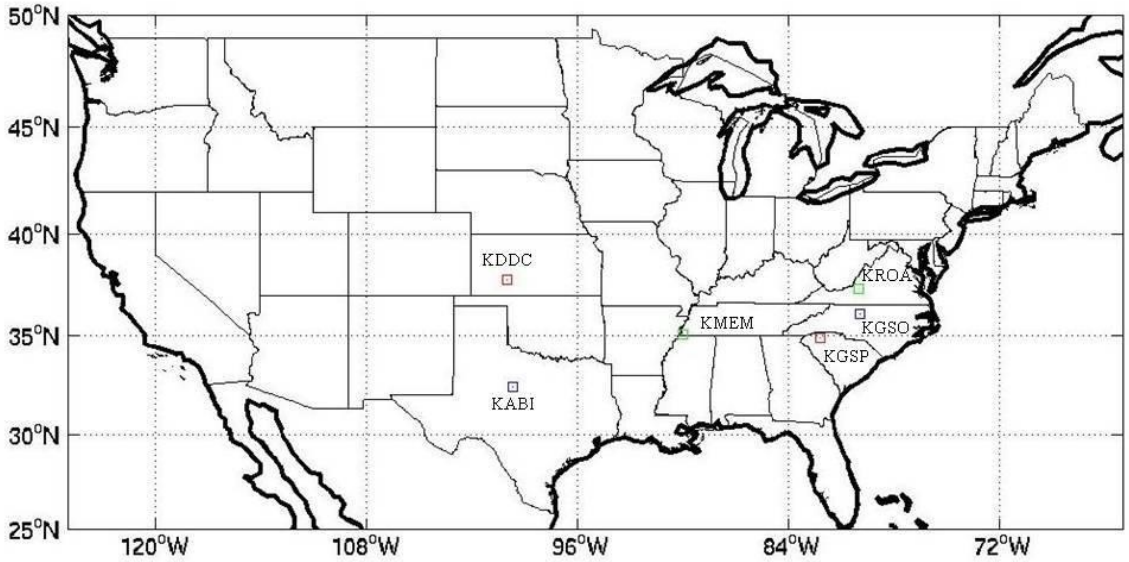

Figure 1 ASOS locations co-located (within 20 miles) with shared grid points.

Several additional analyses were performed among the various datasets to evaluate how each reanalysis represented the particular event in relation to the other reanalyses. In order to make direct comparisons between datasets of differing resolutions

interpolation needed to be performed on the fields of study. Low resolution data were linearly interpolated to the grid points of the higher resolution data to directly contrast the temperature and specific humidity field structures. Differences could then be taken between the two datasets to isolate anomalies linked to the enhanced spatial resolution of the higher resolution reanalyses. To assess the realism of the anomalies in the high resolution datasets, the reanalyses were directly compared to the actual values observed at the various ASOS stations. Reversing the linear interpolations, interpolating from high to low resolution, degraded the high resolution data, to isolate large scale systematic biases in either the temperature or specific humidity fields.

The January 2004 CAO onset was associated with a strong cold front that passed through the Midwest region beginning on January 3rd and continued southeastward, reaching the Atlantic coast by the 6th. The passage of the cold front was examined through difference fields between the MERRA and NCEP datasets using 4x-daily values from both datasets, the results of which will be discussed in the next section. The frontal passage was also tracked through comparisons among the three datasets and ASOS observations for selected cities. Large scale systematic biases were diagnosed using differences between the 4x-daily observations from the NCEP datasets and the corresponding values from MERRA but averaged over the entire month of January. Similarly, monthly diurnal cycles were used to contrast the reanalysis datasets to ASOS observations for particular cities by studying how well the reanalyses represent mean diurnal temperature cycles. The purpose of performing comparative thermodynamic and hydrodynamic analyses for the January 2004 event was to determine which reanalysis

product represents the key synoptic features of the CAO the best. The results of these comparative analyses are presented and discussed in the next section.

CHAPTER 3

RESULTS AND DISCUSSION

3.1 Teleconnections

Cold air outbreaks are influenced by circulations on a variety of length scales and it is important to understand the dynamics behind each contributor to the phenomenon. Starting with large scale circulations, a brief discussion of the teleconnections between the Polar Regions and the midlatitudes will be explored followed by a synoptic overview. Previous research has demonstrated ties between the positive phase of the Pacific-North American (PNA) teleconnection pattern and CAOs occurring in the southeastern United States (Rogers and Rohli 1991; Downton and Miller 1993). The positive phase of the PNA pattern is characterized by an upper tropospheric wave train consisting of a trough south of the Aleutian Islands, a ridge over the intermountain region of North America, and a trough over the southeastern United States (Wallace and Gutzler 1981). The locations of the ridge and trough over the United States allows for lower tropospheric intrusions of cold, dry air masses from Canada into the lower latitudes of North America, perfect for the onset of a CAO. For the January 2004 event, the PNA index, shown in Figure 2a, had a value of 0.41 (calculated index can be found online at http://www.cpc.noaa.gov/products/precip/CWlink/pna/pna.shtml), less than half a standard deviation and despite being in the correct phase it may not have contributed significantly to the CAO onset.

The North Atlantic Oscillation (NAO) dominates the atmospheric variability in the North Atlantic by controlling the strength of the subpolar westerlies (Cellitti et al.

2006). The NAO also impacts broad scale circulation extending from eastern North America through Europe into central Russia (Thompson and Wallace 2001). The positive phase of the NAO is characterized by anomalously low pressure throughout the Arctic region and higher than average pressure in the central Atlantic Ocean contributing to stronger than normal westerly winds in the midlatitudes over the North Atlantic. When the NAO is in the negative phase, both the subtropical highs and Icelandic low are weakened resulting in a more southern Atlantic storm track (Rogers and van Loon 1979). A more southerly storm track allows for strong Canadian flow into the midlatitudes optimal for cold air outbreaks to occur in the eastern half of the United States. The NAO index had a value of -0.29 (calculated index can be found online at http://www.cpc.noaa.gov/products/precip/CWlink/pna/nao.shtml), as depicted in Figure 2b, in January 2004, but even though it was in the negative phase it may not have contributed significantly to the onset of the CAO.

The location and movement of the cold polar air masses can also be strongly connected to anomalies in a broader atmospheric teleconnection pattern, the Arctic Oscillation (AO). The AO is in the negative or cool phase when a pattern of higher than normal atmospheric pressure resides over the Arctic region causing a weakening of the westerly jet stream in the upper atmosphere. With Arctic high pressure and weak westerlies, cold Arctic air is no longer confined to its origin and can more easily migrate to lower latitudes eventually leading to CAOs for middle latitudes. Conversely, when the Arctic Oscillation is in the positive phase the westerly jet stream is enhanced and polar air masses are confined to high latitudes (Thompson and Wallace 1998). In January 2004 the AO index, shown in Figure 2c, had a value of -1.686 (calculated index can be found

online at http://www.cpc.noaa.gov/products/precip/CWlink/daily_ao_index/ao.shtml), more than one and a half standard deviations below normal. The AO index value is more substantial than either the PNA or NAO and since it is in the negative phase it is probably the most influential teleconnection pattern for this event. Nonetheless, the PNA and to a lesser extent, the NAO are also of the proper phase to promote the onset of a CAO. Therefore, it is important to study and understand the large scale patterns governing the atmospheric variability of the Atlantic Ocean when discussing the circulation behind the movement of polar air masses into the midlatitudes.

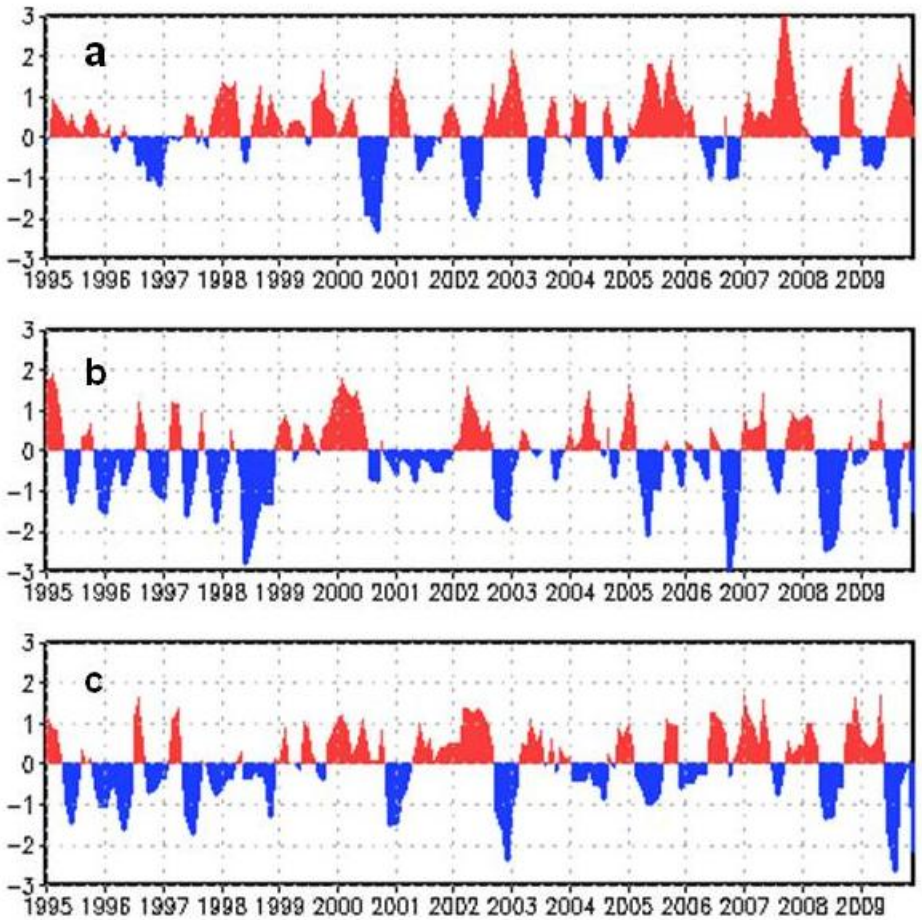

Figure 2 Standardized three-month running mean for a) PNA, b) NAO, and c) AO indices. The standardized departures are calculated using the 1950-2000 base period statistics. (Courtesy of the NWS CPC)

3.2 Synoptic Overview

The teleconnection patterns discussed above influence the synoptic scale features that are characteristic of CAOs, and before studying how the reanalysis datasets represent the synoptic features it is useful to present an overview of the salient synoptic features involved. Maximum and minimum temperature maps from the NCEP Hydrometeorological Prediction Center (HPC) for January 5th and 7th are presented in Figure 3 to demonstrate the effects of the CAO on the middle latitudes associated with a cold frontal passage. Before the onset of the CAO, the southeast had maximum daily temperatures in the seventies and eighties and minimum daily temperatures in the fifties and sixties, but two days after the passage of the cold front the region observed maximum daily temperatures twenty to thirty degrees cooler and minimum daily temperatures forty degrees cooler. Aside from Florida, the southeastern United States experienced dramatic cooling in only two days. The considerable drop in temperatures from the southeast to the Missouri Valley could be the result of cold polar air migration.

The MERRA dataset accurately depicts the location and advection of the cold, Canadian air in Figure 4 where surface air temperature is displayed with surface wind vectors overlain for 12z on January 5, 2004. The large temperature gradient of approximately forty degrees between the southeastern United States and the cold pool in Canada agrees well with the observational analyses found in the temperature maps just described. The pool of cold air is beginning to infiltrate down into the upper Midwest of the United States and will soon impact the lower portion of the United States in association with strong northerly and northwesterly flow. A similar wind and temperature pattern exists at 850 hPa depicted in Figure 5 demonstrating the depth of the

cold pool located in central Canada, a key ingredient for the CAO that impacted the Deep South in the following hours.

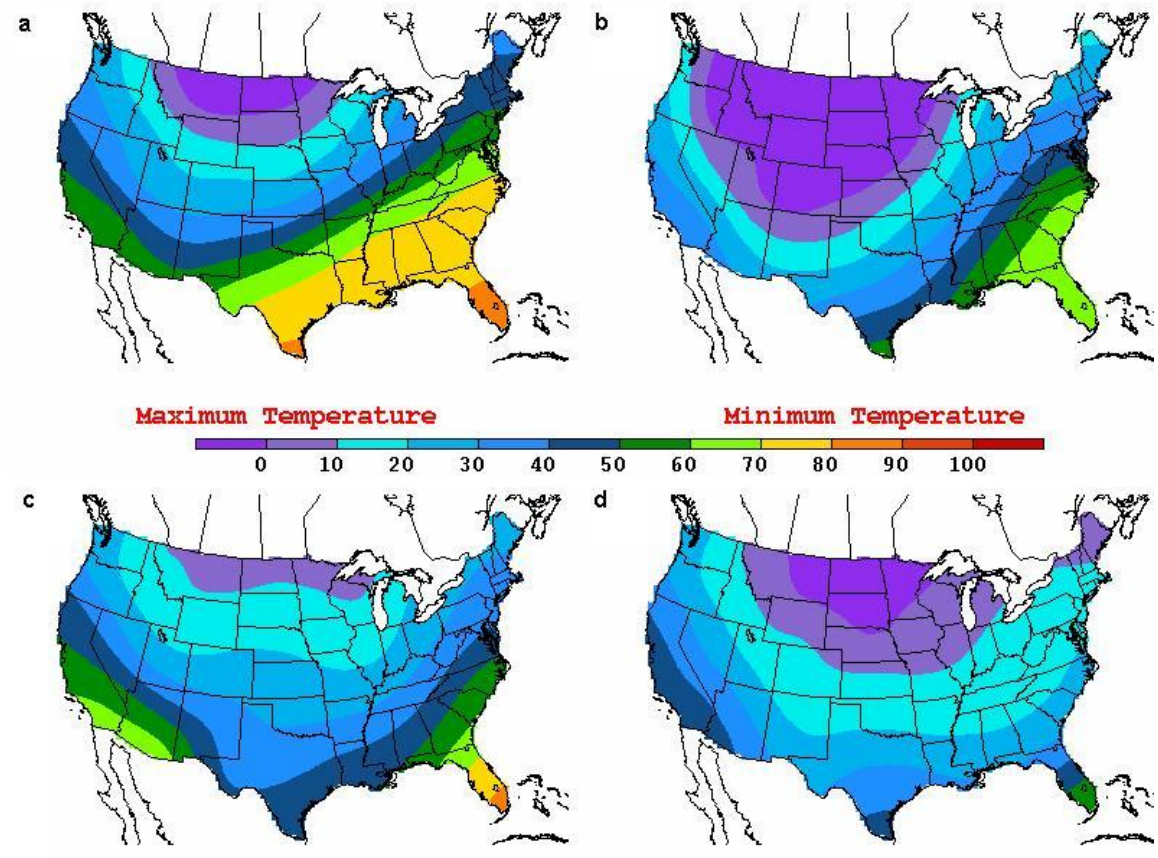

Figure 3 Maximum and minimum temperature maps for January 5, 2004 (a, b) and January 7, 2004 (c, d). (NCEP HPC)

The weather map displayed in Figure 6 from the National Weather Service (NWS) Hydrometeorological Prediction Center (HPC) contains information about the surface and station weather that occurred on the morning of January 5th. At 12z when the map was analyzed, the cold front associated with CAO onset is located along the border between Tennessee and North Carolina extending north to eastern West Virginia and southwest to southeastern Louisiana. The cold front is connected to a low pressure

system centered over the Mid-Atlantic States, providing an area with precipitation prior to the surge of cold air migrating down from central Canada. The combination of cyclonic flow around the low and anticyclonic flow around the high pressure to the west and north provided ideal conditions for the cold, Canadian air to migrate into the Midwestern United States and eventually the Deep South. The northerly and northwesterly flow shown in Figures 4 and 5 correspond to flow between the high pressure and low pressure systems illustrated in Figure 6 providing evidence that the MERRA reanalysis dataset represents synoptic scale features appropriately.

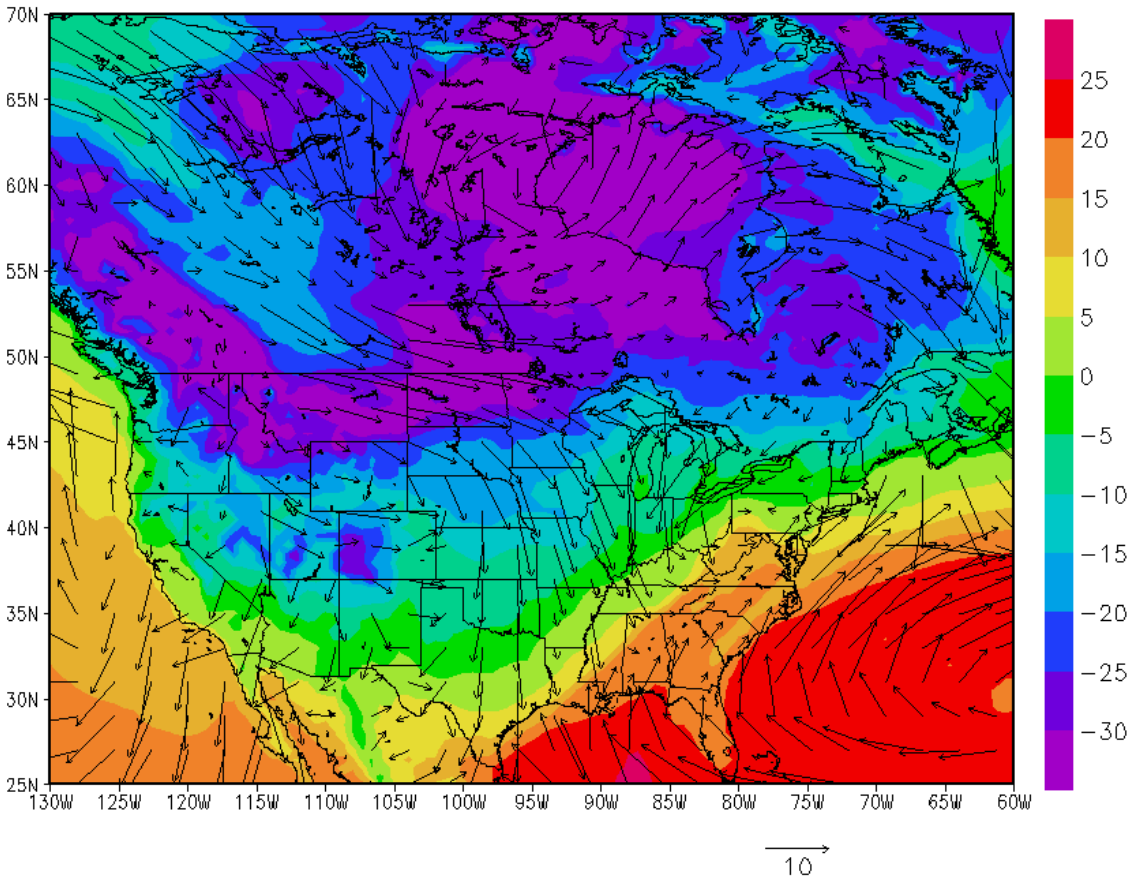

Figure 4 MERRA 2m temperature (shading) and wind (vectors) for 12z January 5, 2004. Color bar shading interval in degrees Celsius and a scale wind vector are provided.

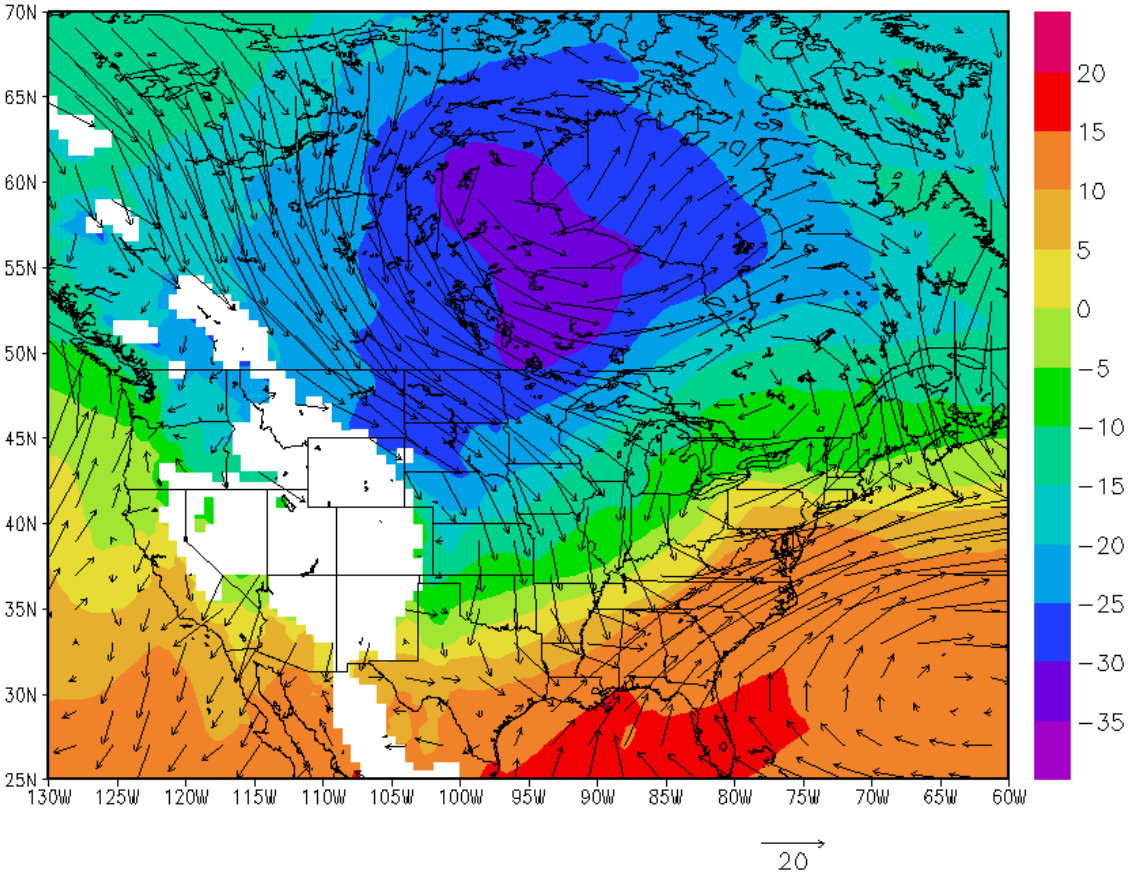

Figure 5 MERRA 850 hPa temperature (shading) and wind (vectors) for 12z January 5, 2004. Color bar shading interval in degrees Celsius and a scale wind vector are provided.

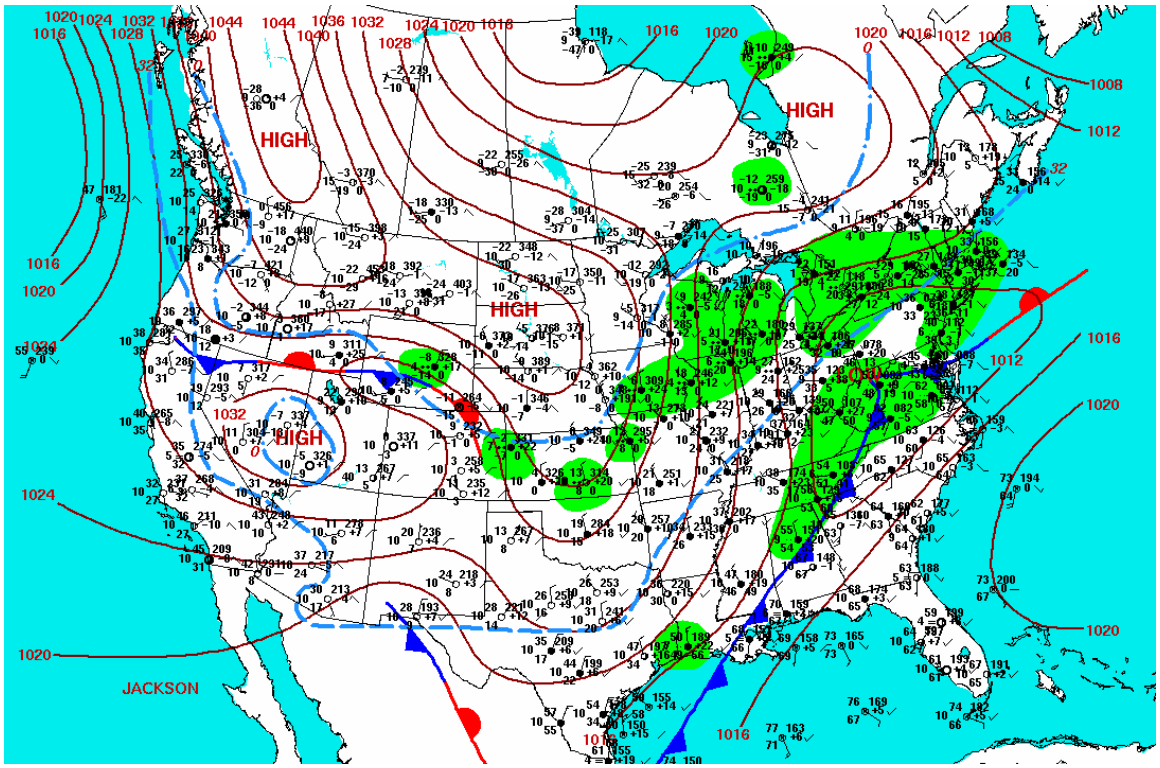

Figure 6 Analyzed surface weather map with plotted station observations. (NCEP HPC)

3.3 Dataset Intercomparisons

Comparisons between the MERRA and NCEP datasets reveal small scale frontal features with the January 2004 CAO event. Examination of the surface temperature difference field between MERRA and NCEP, linearly interpolated to the MERRA grid, displays a linear dipole of strong cold anomalies northwest of weak warm anomalies at 12z on January 5th as displayed in the top panel of Figure 7. The temperature anomaly gradient is collocated with the cold front found on the corresponding surface map analysis from HPC (Figure 6). The warm anomalies lie along an area of precipitation from West Virginia to Alabama and the cold anomalies are consistent with colder temperatures observed at ASOS stations after the passage of the cold front. Following the movement of the linear dipole of warm and cold anomalies through 18z on the 5th and 00z on the 6th, middle and bottom panels of Figure 7 respectively, the cold front connected to the CAO can be tracked as it traveled eastward in a twelve hour period. Aside from the frontal passage, the temperature field maps show a cooler eastern United States at 12z compared to a substantially warmer pattern at 18z.

Surface specific humidity analyses, similar to Figure 7, for the period from 12z January 5th (top panel) to 00z January 6th (bottom panel) are displayed in Figure 8. The specific humidity difference fields reveal a linear dipole in moisture anomalies with strong positive anomalies where precipitation is located on the surface map analysis from Figure 6 and negative anomalies downstream of the front. The boundary between the opposing anomaly regions corresponds to the location of the cold front (Figure 6). As for the temperature difference maps, the passage of the front can be monitored using the movement of the linear moisture dipole illustrated in the specific humidity difference

maps through 00z January 6th, the bottom panel of Figure 8. In addition to the location of the cold front, the 12z map exhibits an overall dry anomaly while 00z is characterized by anomalously high moisture throughout the Mid-Atlantic portion of the country. The difference fields between MERRA and NCEP for temperature and specific humidity exhibit important characteristics related to the cold frontal passage associated with the CAO onset. MERRA is colder and drier than NCEP behind the front, but warmer and wetter ahead of the front indicating a difference in estimation of the thermal and moisture gradients associated with the mesoscale components of the frontal feature. The performance of the different datasets for individual cities impacted by the passage of the front will be investigated next.

The detailed structure of the cold front passage was studied through comparisons of the time series obtained from the reanalyses (MERRA, NCEP, and NARR) and local ASOS observations. The purpose of the time series analyses was to uncover possible limitations in the reanalysis datasets. At 12z in Figure 6 the front was located at the border between Tennessee and North Carolina so it had already passed over KMEM. Looking at the corresponding time series for KMEM, presented in Figure 9, it is clear that both MERRA and NARR capture the daily diurnal cycle better than NCEP prior to the cold frontal passage while performing equally well at 12z on January 5th. After the passage of the front, both MERRA and NARR become warmer than NCEP as was seen in the temperature difference fields between MERRA and NCEP in Figure 7. The time series analysis for KGSO is shown in Figure 10 for 06z January 5th through 06z January 7th to represent the cold front movement through North Carolina. Different from the KMEM time series, all the reanalysis datasets perform equally well in comparison to

ASOS observations with an exception at 18z January 6th where NCEP is several degrees cooler than the other reanalyses and observations. Correlations were calculated for the period from 06z on January 3rd through 06z on the 7th to include the frontal passage over both cities to determine which reanalysis product performed the best overall. Table 1 shows MERRA is highly correlated with ASOS for both cities with NARR and NCEP having correlations of 0.98 at KMEM. Despite a lesser correspondence for KGSO, NCEP still had a high correlation with the ASOS temperature observations.

Table 1 Temperature correlations with ASOS for 06z January 3 to 06z January 7

Reanalysis Product	KMEM (Memphis, TN)	KGSO (Greensboro, NC)
MERRA	0.99	0.98
NARR	0.98	0.97
NCEP	0.98	0.93

Similarly, moisture time series were compared among the reanalysis datasets and the ASOS observations. Beginning with the KMEM time series depicted in Figure 11, all three reanalyses are generally wetter than the ASOS observations with NCEP being anomalously moist at 12z on both days prior to the frontal passage. These signatures are important to note since NCEP peaks in moisture content while MERRA and NARR experience corresponding drops in specific humidity. With the advance of the cold front, the specific humidity values drop due to the advection of dry air into the region. After the passage of the cold front, all three reanalyses capture the lack of moisture equally well suggesting greater performance when moisture levels are low. Overall, the reanalyses are highly correlated to ASOS observations as shown in Table 2 with MERRA

slightly better than NARR. Similar results are found in the specific humidity time series for KGSO shown in Figure 12, specifically the moisture peak in the lower resolution NCEP at 12z prior to the cold front passage. Just like at KMEM, the reanalyses are better correlated to the ASOS values once dry air has been advected into the area after the cold front has passed. Both MERRA and NARR are highly correlated to ASOS values, but NCEP has a correlation of only 0.86 possibly due to the lower resolution of the reanalysis.

Table 2 Specific humidity correlations with ASOS for 06z January 3 to 06z January 7

Reanalysis Product	KMEM (Memphis, TN)	KGSO (Greensboro, NC)
MERRA	1.00	0.96
NARR	0.99	0.96
NCEP	0.96	0.86

The final set of dataset comparisons performed involved monthly averages of temperature and specific humidity to determine if signatures found in the difference fields and time series are the result of systematic biases in either MERRA or NCEP. Biases were diagnosed through the use of monthly mean temperature and specific humidity difference field maps along with diurnal cycle time series for individual cities similar to the comparisons discussed above. Monthly mean temperature difference field maps are shown in Figure 13, where the difference between MERRA and NCEP interpolated to the MERRA grid is displayed on a map of the continental United States for 00z, 06z, 12z, and 18z since NCEP has limited temporal resolution. MERRA tends to be slightly cooler than NCEP over the continental United States during the evening hours of the day as

shown by the 00z and 06z difference fields, Figure 13a and b respectively. Sparse warm anomalies exist in the western portion of the United States at 00z becoming enhanced by 06z while most of the cooler anomalies in the eastern part of the country disappear in those six hours. Comparison of the 06z and 12z maps, Figures 13b and c, show only slight changes with slight enhancements occurring in the western part of the country. By 18z, illustrated in Figure 13d, at which time strong solar heating occurs and prominent warm anomalies cover most of the country especially in the southwest United States with differences near 10 K.

Monthly mean temperature diurnal cycle time series were created for KMEM and KGSO, shown in Figures 14 and 15 correspondingly. Both time series reveal significant differences in value between NCEP and the other three datasets at 18z since NCEP does not exhibit a local temperature peak like MERRA, NARR, and ASOS do, providing strong evidence for a systematic 18z cold bias in NCEP. Table 3 presents the resultant correlations between the reanalysis datasets and ASOS observations revealing that NCEP inadequately captures the daily diurnal cycle at KMEM and KGSO for January 2004. On the other hand, MERRA handles the diurnal temperature cycle well while NARR achieved even better correlation for the month at both KMEM and KGSO.

Table 3 Monthly mean temperature correlations with ASOS for January 2004

Reanalysis Product	KMEM (Memphis, TN)	KGSO (Greensboro, NC)
MERRA	0.97	0.96
NARR	1.00	0.99
NCEP	0.80	0.92

Monthly mean specific humidity difference field maps for January 2004 were also created to diagnose any potential moisture biases that might exist in the various reanalysis datasets. The specific humidity monthly mean difference field maps presented in Figure 16 display the differences between MERRA and NCEP interpolated to the MERRA grid for 00z, 06z, 12z, and 18z averaged over the month of January 2004. Positive anomalies are observed west of the Rocky Mountain range while negative anomalies appear along the southeast coast of the United States at 00z, Figure 16a. The transition from 00z to 06z displays a weakening of the wet anomalies in the west and a slight increase of dry anomalies across the country as a whole. By 12z displayed in Figure 16c, the MERRA dataset becomes significantly drier than the NCEP dataset across the whole country particularly over the southeast. The 18z difference field presented in Figure 16d displays a general decrease in the magnitude of the negative anomalies with the strongest differences occurring along the Gulf Coast, the southeast coastline, and the far northeast corner of New Mexico.

The moisture diurnal cycle time series for KMEM and KGSO illustrated in Figures 17 and 18 were also performed to test how the three datasets performed in comparison to the ASOS observations. Both higher resolution reanalyses, MERRA and NARR, have a moist bias throughout the entire month, but it would appear NARR may have a better diurnal cycle. The correlations between the reanalyses and ASOS observations is presented in Table 4 showing that NARR outperformed MERRA and NCEP at KMEM while MERRA performed slightly better than NARR for KGSO. The moisture bias at 12z in the NCEP dataset seen in the cold frontal passage time series also appears in the diurnal cycle time series with a substantial bias of almost 0.002 kg/kg at

12z. The negative correlation for KMEM reflects this well and although a negative correlation is not shown for KGSO, it is a very weak positive correlation at that. The observed diurnal cycle in moisture for both stations is considerably weaker than represented in any of the three reanalyses indicating the general difficulty in capturing the actual moisture values observed at the ASOS station location.

Table 4 Monthly mean specific humidity correlations with ASOS for January 2004

Reanalysis Product	KMEM (Memphis, TN)	KGSO (Greensboro, NC)
MERRA	0.77	0.89
NARR	0.99	0.87
NCEP	-0.32	0.13

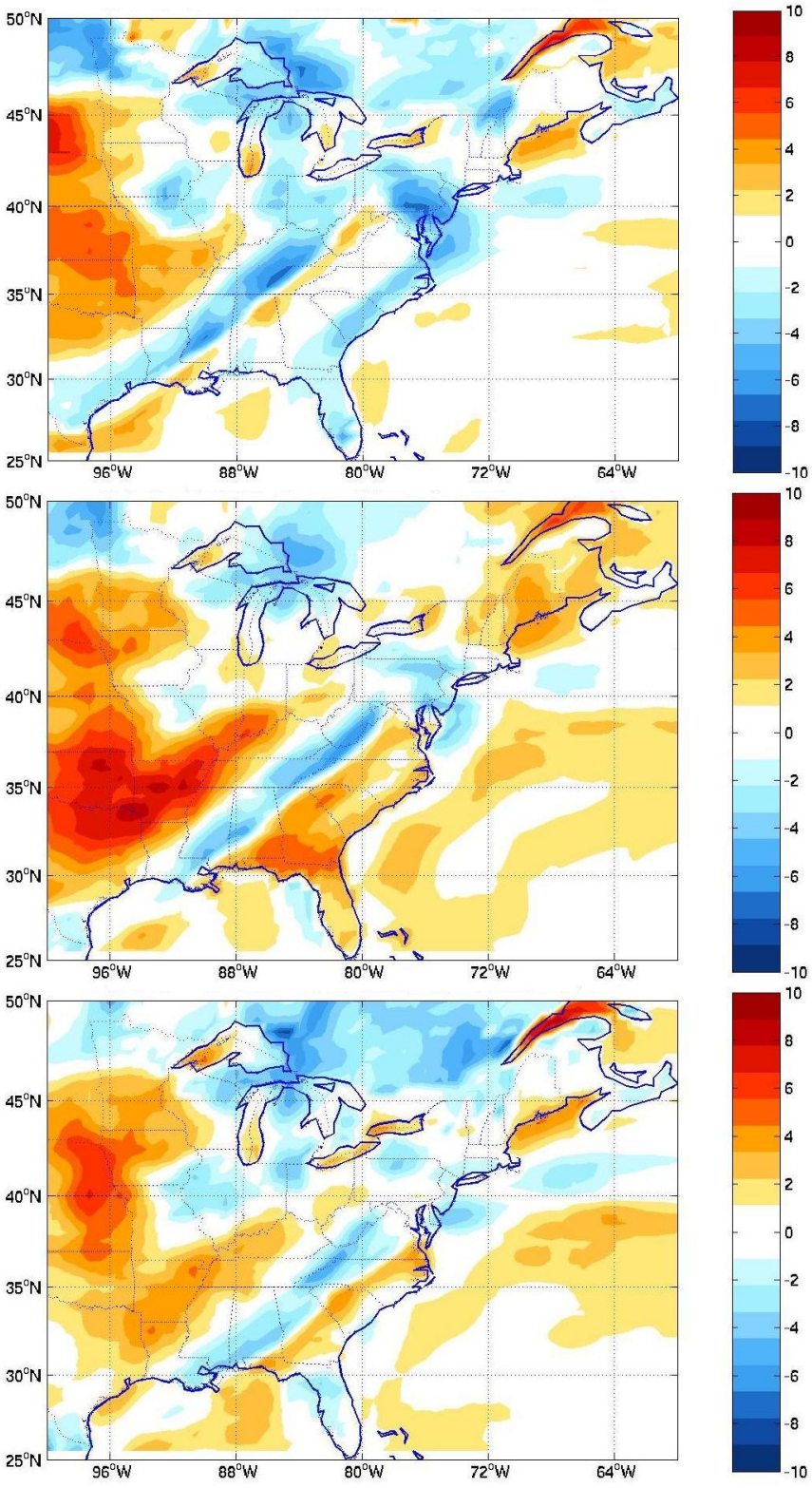

Figure 7 Surface temperature difference fields (MERRA - NCEP) for 12z January 5 (top), 18z January 5 (middle), and 00z January 6 (bottom) 2004. NCEP was interpolated to MERRA before difference was taken. Color bar depicts shading interval in degrees Celsius.

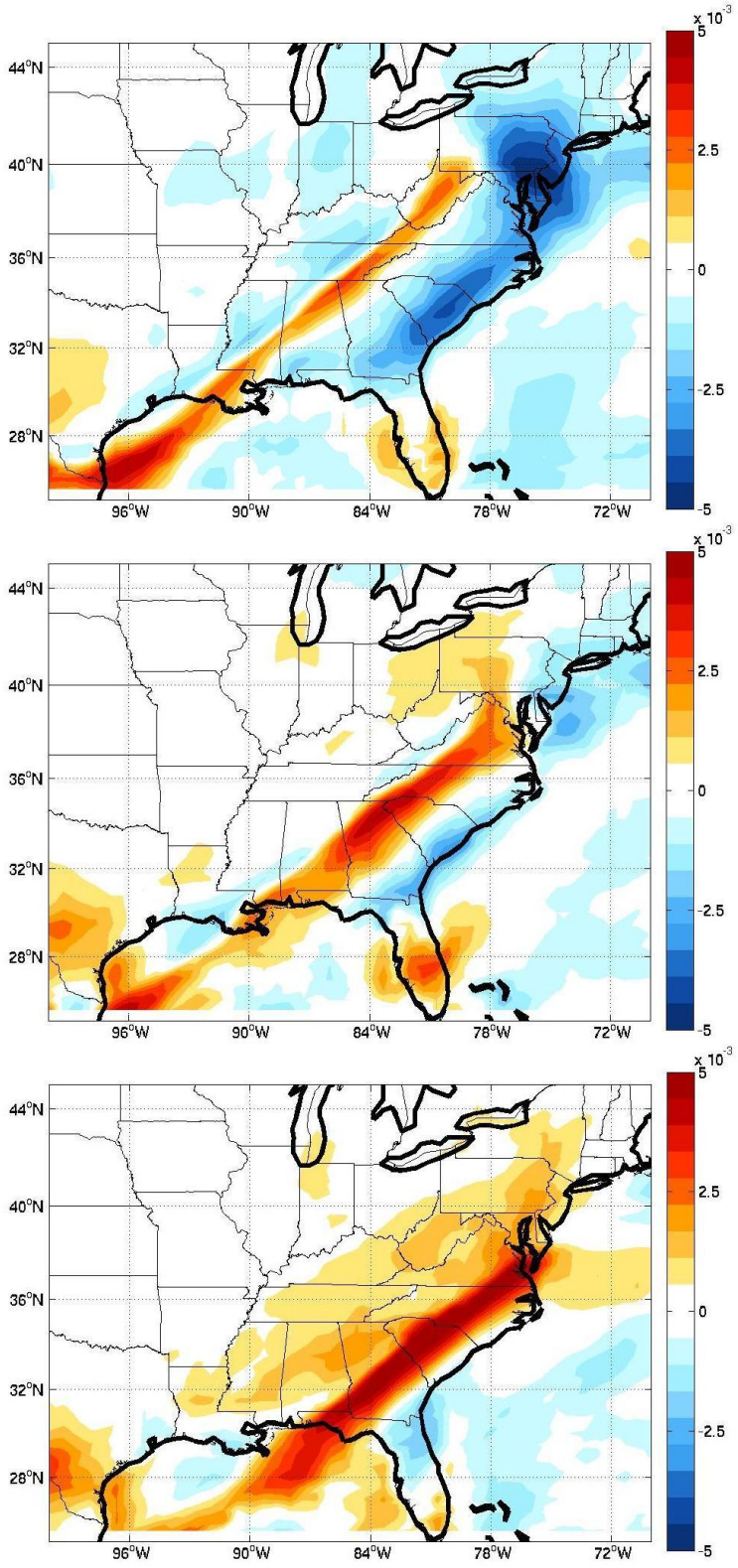

Figure 8 Surface specific humidity difference fields (MERRA - NCEP) for 12z January 5 (top), 18z January 5 (middle), and 00z January 6 (bottom) 2004. NCEP was interpolated to MERRA before difference was taken. Color bar depicts shading interval in kg/kg.

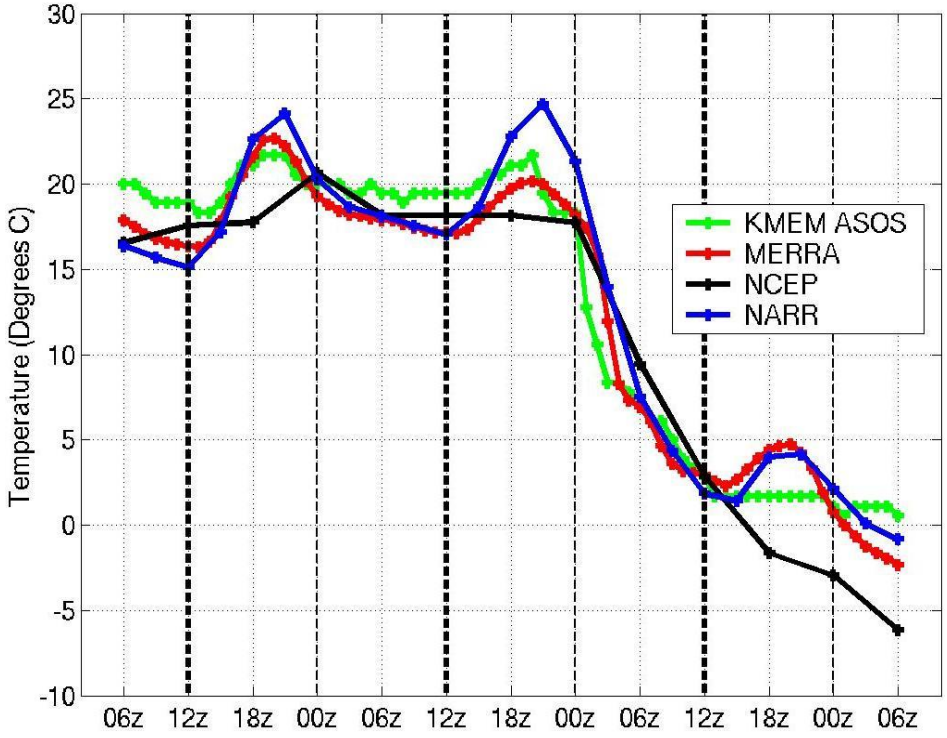

Figure 9 KMEM temperature time-series for frontal passage from 06z January 3 to 06z January 6.

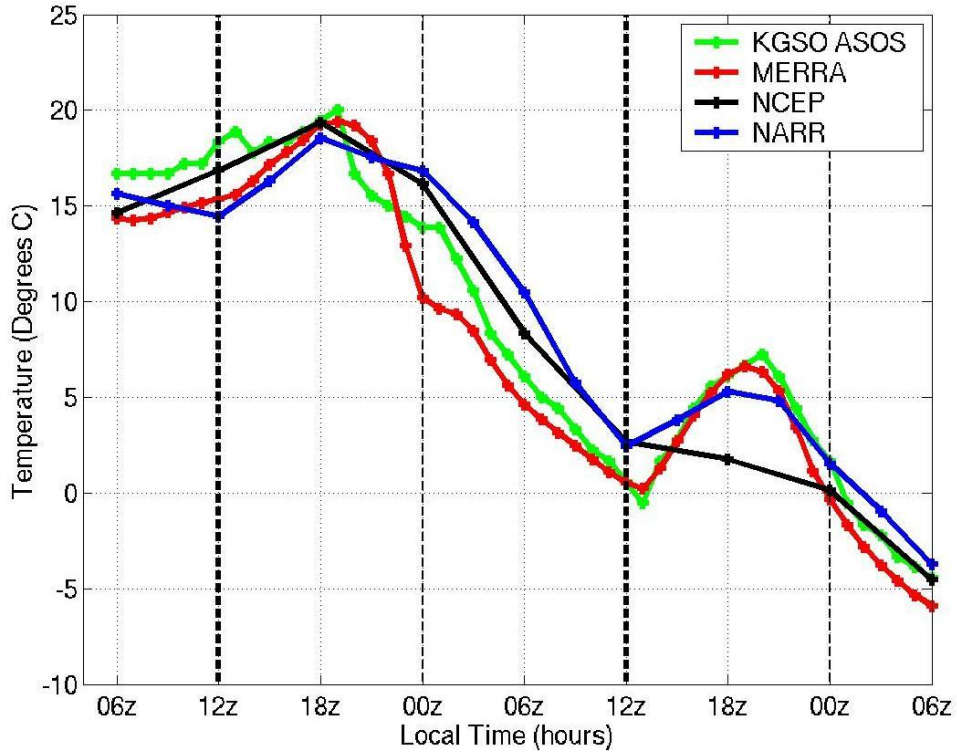

Figure 10 KGSO temperature time-series for frontal passage from 06z January 5 to 06z January 7.

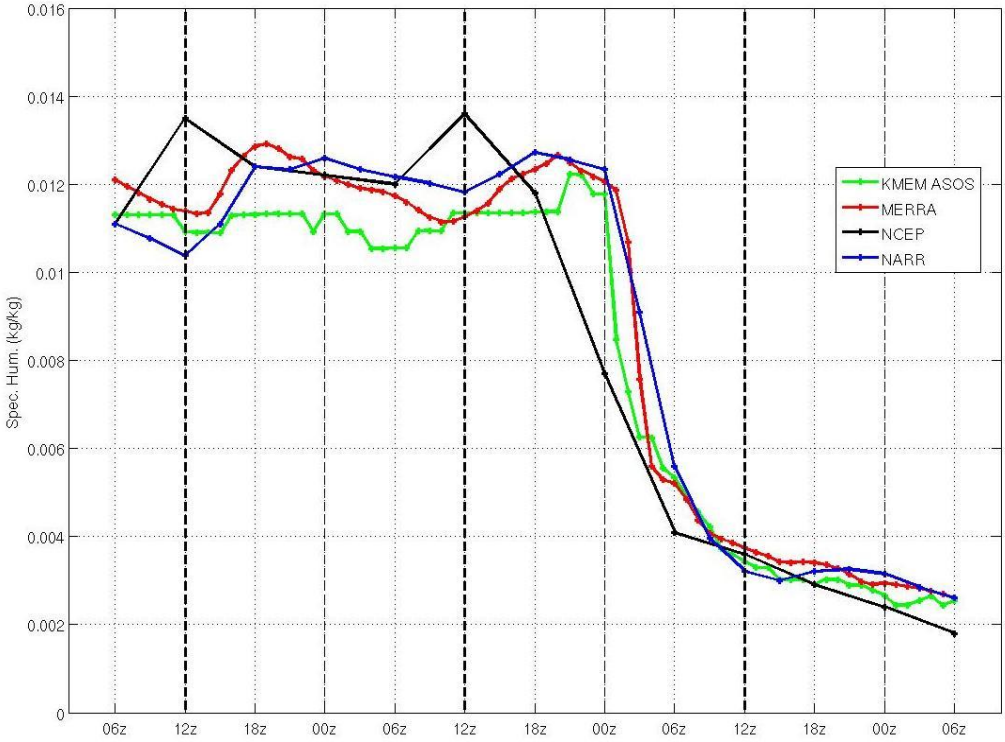

Figure 11 KMEM surface specific humidity time series for 06z January 3 to 06z January 6.

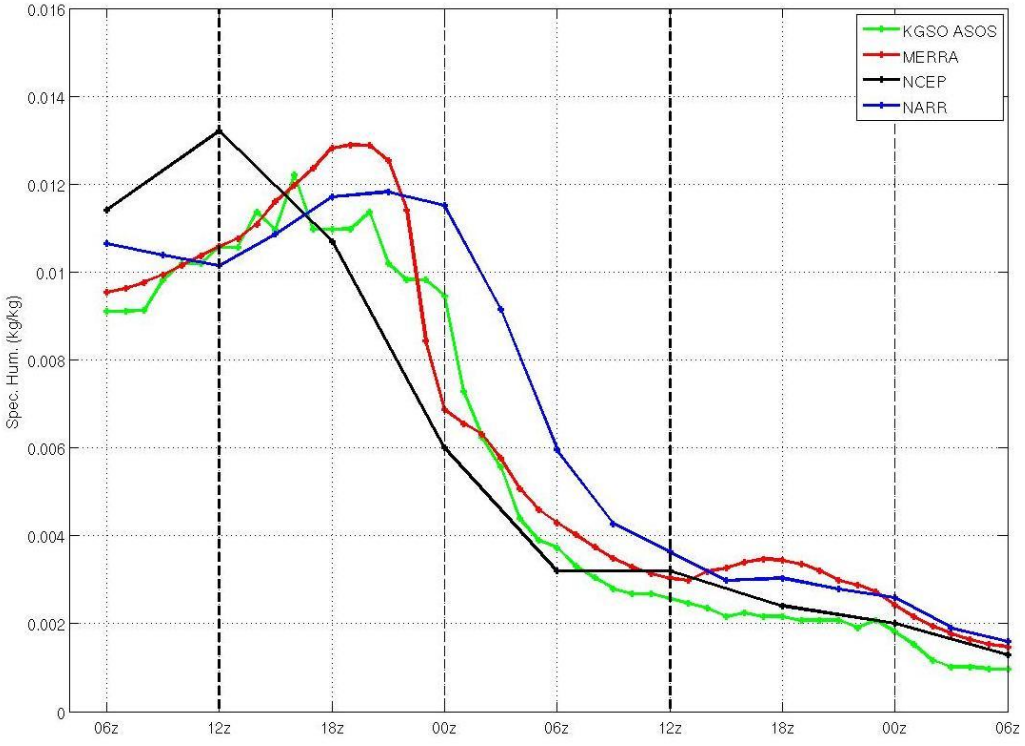

Figure 12 KGSO surface specific humidity time series for 06z January 5 to 06z January 7.

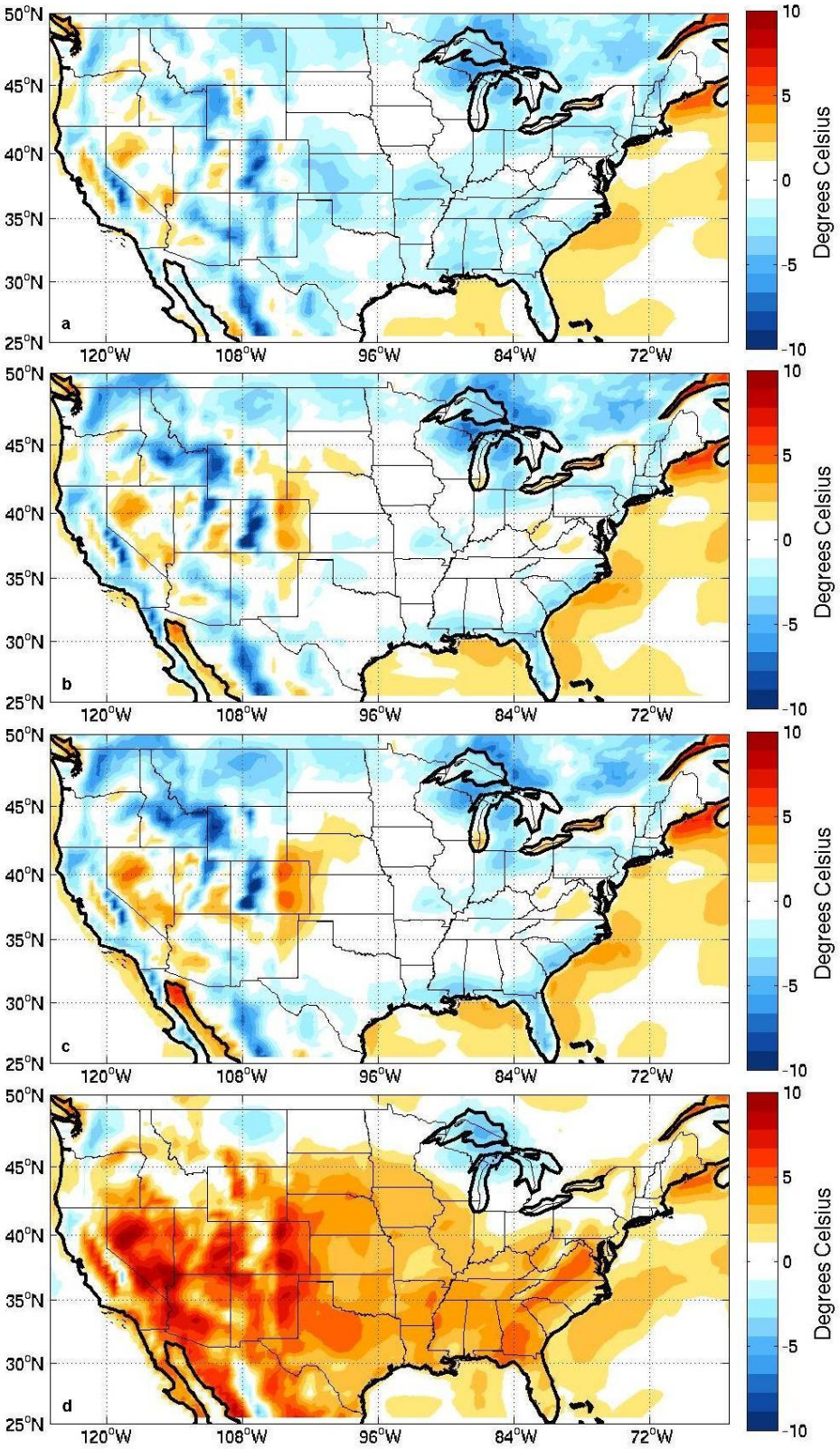

Figure 13 Monthly mean temperature difference fields (MERRA – NCEP) for a) 00z, b) 06z, c) 12z, and d) 18z. NCEP was interpolated to MERRA before difference was taken.

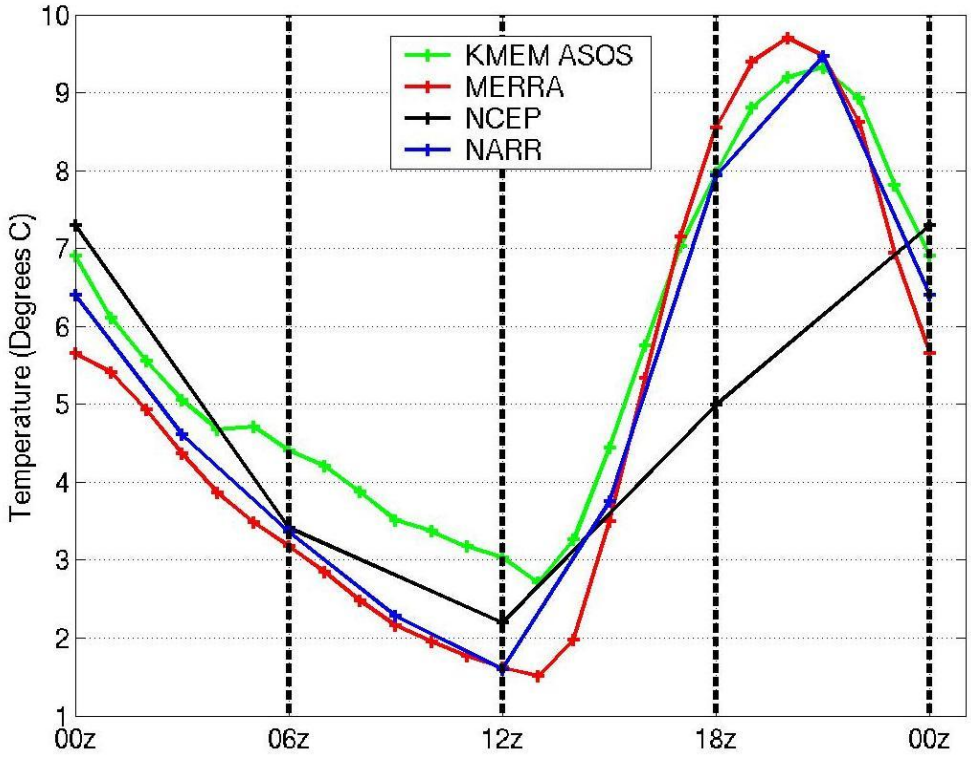

Figure 14 Monthly mean surface temperature diurnal cycle for KMEM.

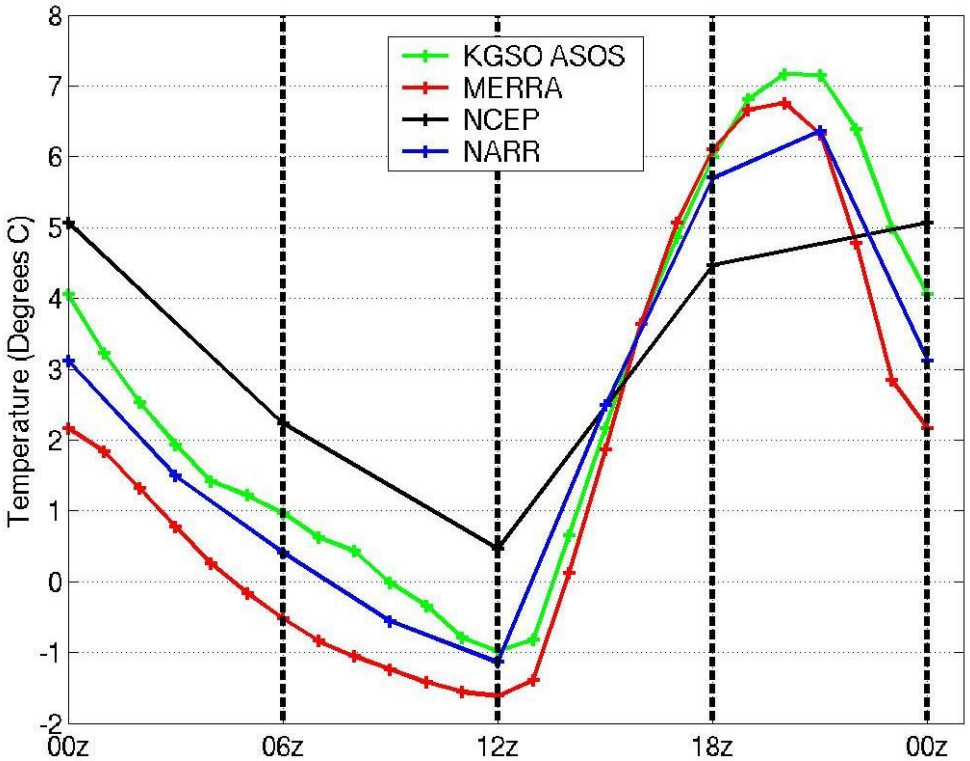

Figure 15 Monthly mean surface temperature diurnal cycle for KGSO.

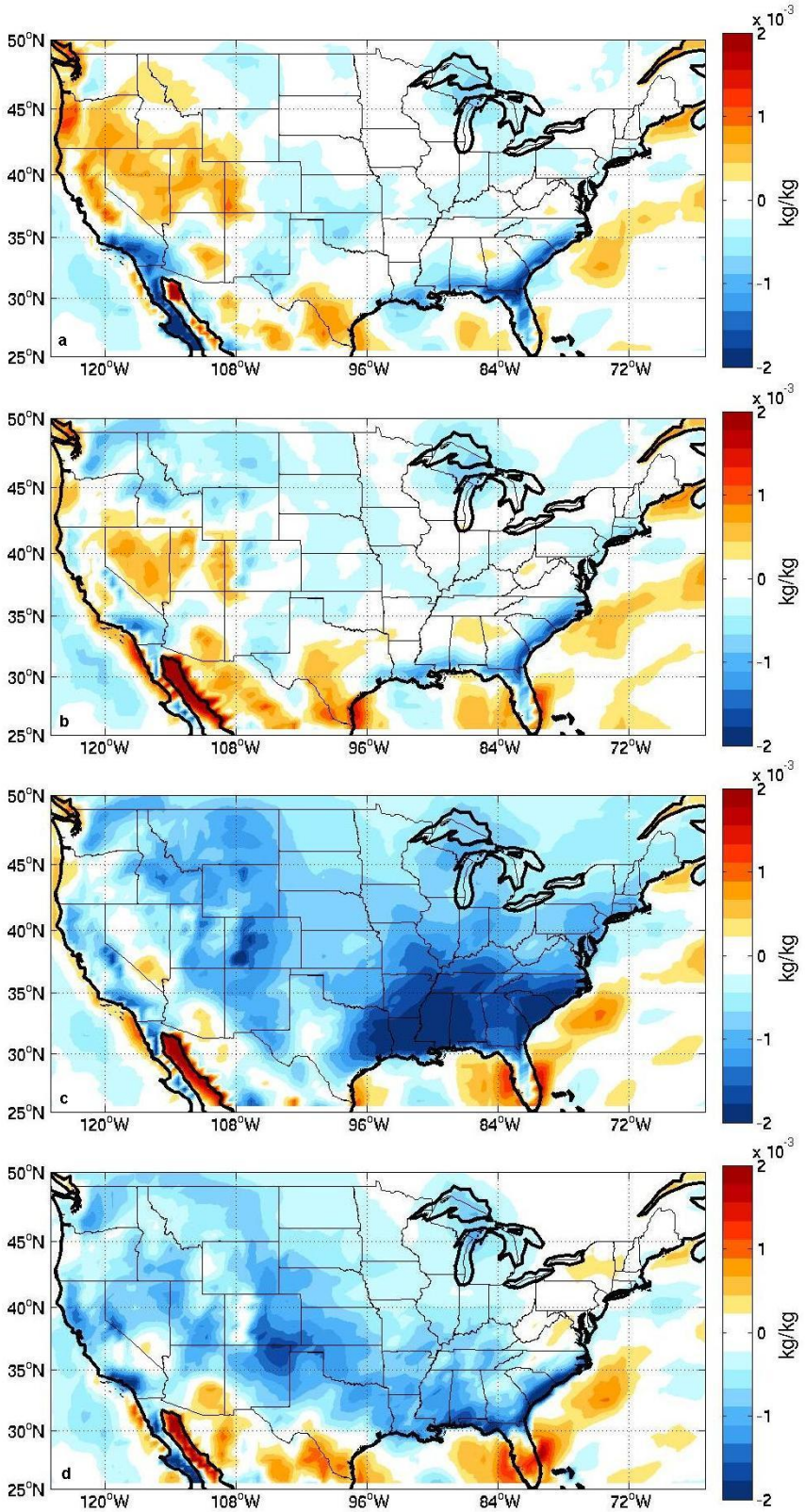

Figure 16 Monthly mean specific humidity difference fields (MERRA – NCEP) for a) 00z, b) 06z, c) 12z, and d) 18z. NCEP was interpolated to MERRA before difference was taken.

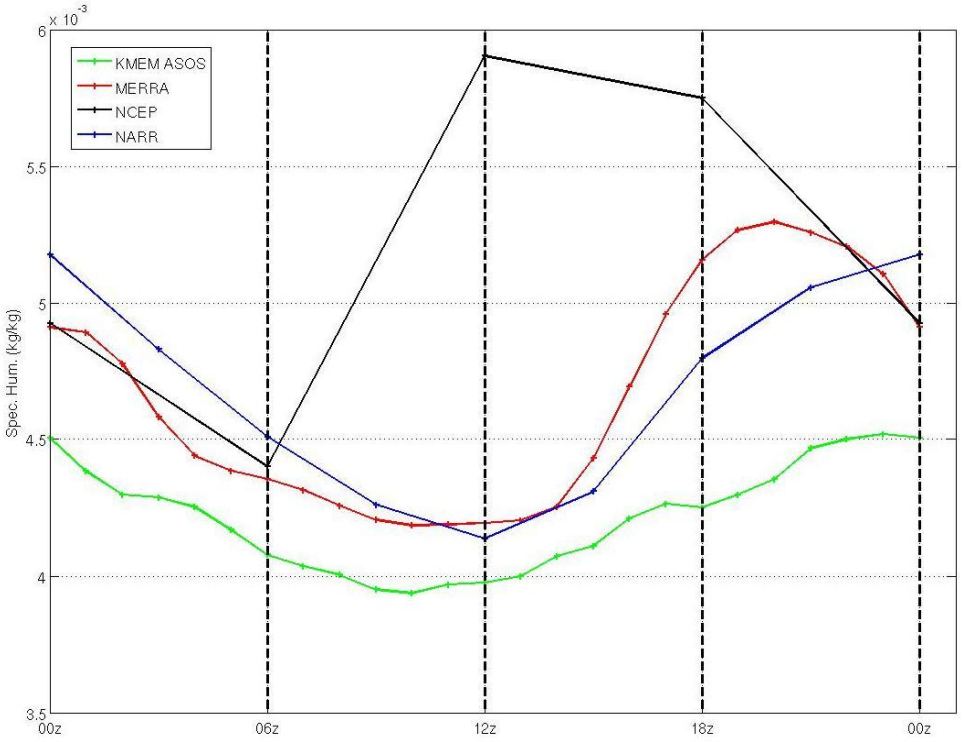

Figure 17 Monthly mean surface specific humidity diurnal cycle time series for KMEM.

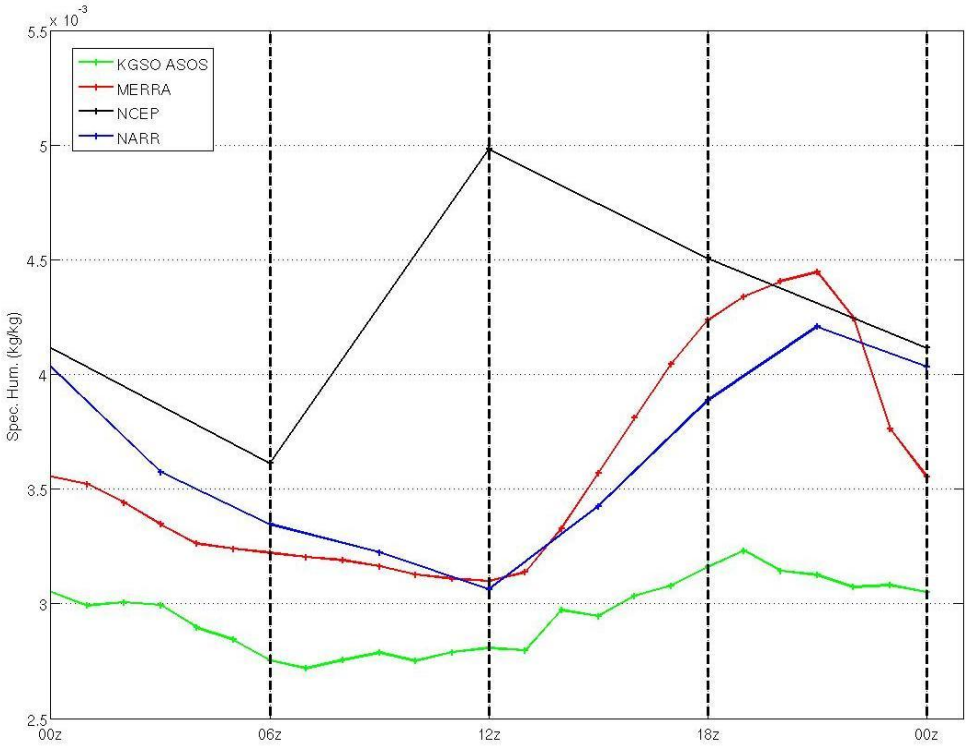

Figure 18 Monthly mean surface specific humidity diurnal cycle time series for KGSO.

3.4 Dynamical Analyses

The final set of analyses performed were the three-dimensional structural analyses of the Ertel potential vorticity (EPV) fields from the MERRA reanalysis dataset. Two-dimensional fields for 850 hPa (Figure 19) and 500 hPa (Figure 20) are plotted to determine which atmospheric levels exhibited notable potential vorticity (PV) structures during the CAO. Prominent PV maxima were observed at 850 hPa and 500 hPa over central Canada and the Great Lakes with the largest amplitudes at the 500 hPa level. The central Canadian PV maximum shows less vertical phase tilt than the Great Lakes' PV maximum which exhibits a slight northwest tilt with height, but appears to be the more influential feature for the event in question. The PV maximum located in the eastern United States at 850 hPa in Figure 19 displays PV anomalies along the frontal boundary seen in Figure 7 contributing to the movement of the front. The two lower and middle tropospheric PV features are dynamically linked to the circulation pattern of the lower troposphere influencing the movement of the cold front associated with CAO onset.

Vertical cross sections were created using the same data used to create the two-dimensional fields, but for a latitudinal slice through the atmosphere from the surface up to 250 hPa. The central Canadian feature was captured using the latitude of 60°N displayed in Figure 21 while the Great Lakes' PV maximum is closer to the latitude of 45°N shown in Figure 22. Examination of the vertical cross sections for both PV features revealed similarities with a magnitude between 8 and 9 potential vorticity units (PVU) at 250 hPa and depth throughout the atmosphere from approximately 600 hPa to 250 hPa, but the Great Lakes' maximum is consistent with the existence of a tropopause fold at the longitude corresponding to the location of the cold front associated with the CAO onset.

A tropopause fold occurs when stratospheric air and higher potential vorticity is pulled down into the troposphere characterized by lower potential vorticity (Rao et al. 2008). Potential vorticity is a dynamical parameter that measures, in part, the stratification of isentropic temperature surfaces in the vertical. When a tropopause fold occurs, isentropic surfaces are stretched vertically causing a corresponding destabilization of the upper atmosphere and the local generation of geostrophic relative vorticity, spinning up a cyclonic circulation around the region of the fold (Danielsen 1968). The induced circulation occurring at 45N, 80-85W is evident in Figures 4 and 5 through the examination of the circulation of the near-surface and 850 hPa winds. Therefore, the tropopause fold displayed in the vertical cross section of PV corresponding to 45°N depicted in Figure 22 likely helped to contribute to the favorable conditions for the CAO onset to occur.

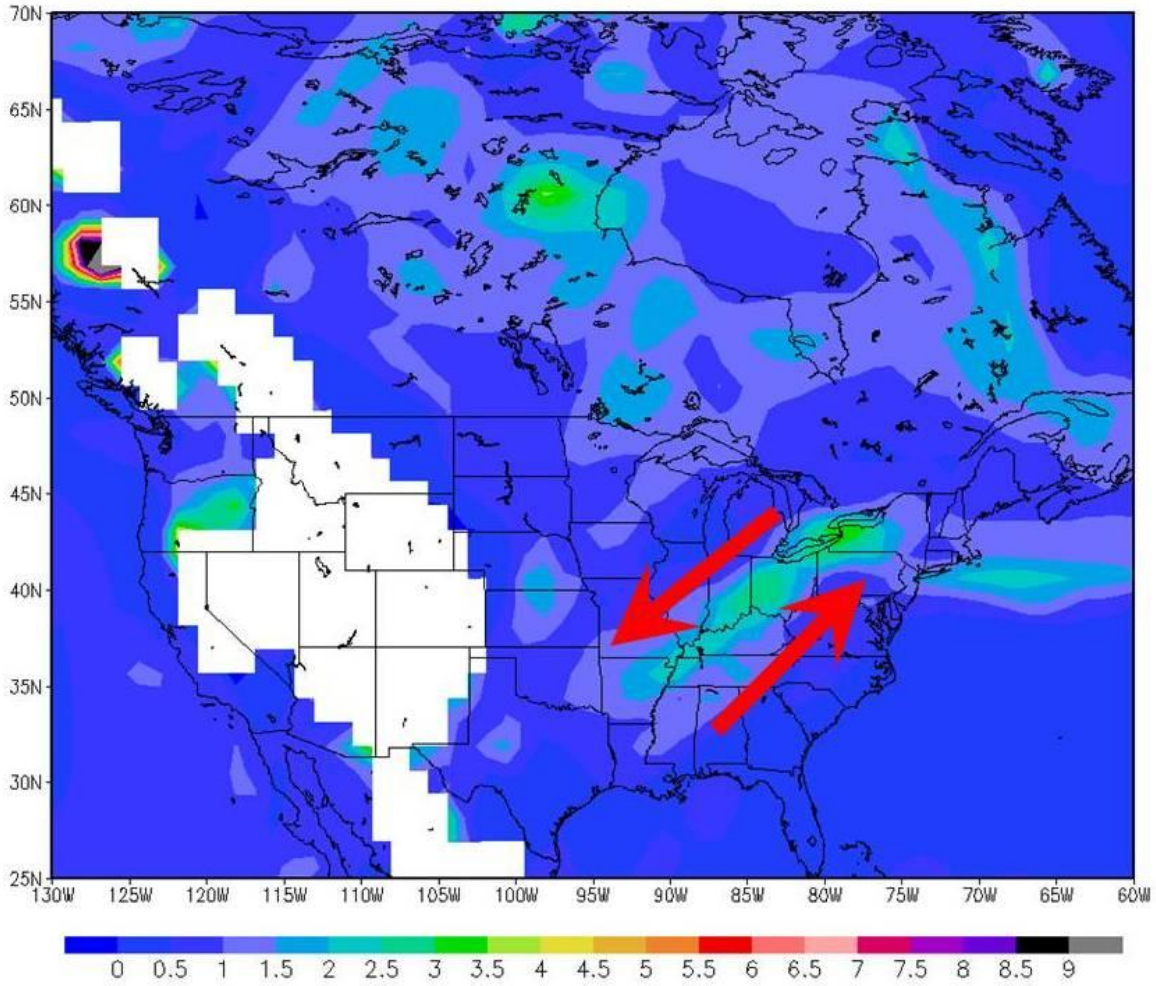

Figure 19 850 hPa MERRA Ertel Potential Vorticity field for 12z January 5. Color bar shading indicates values in potential vorticity units (PVU). Red arrows illustrate circulation induced by PV maximum.

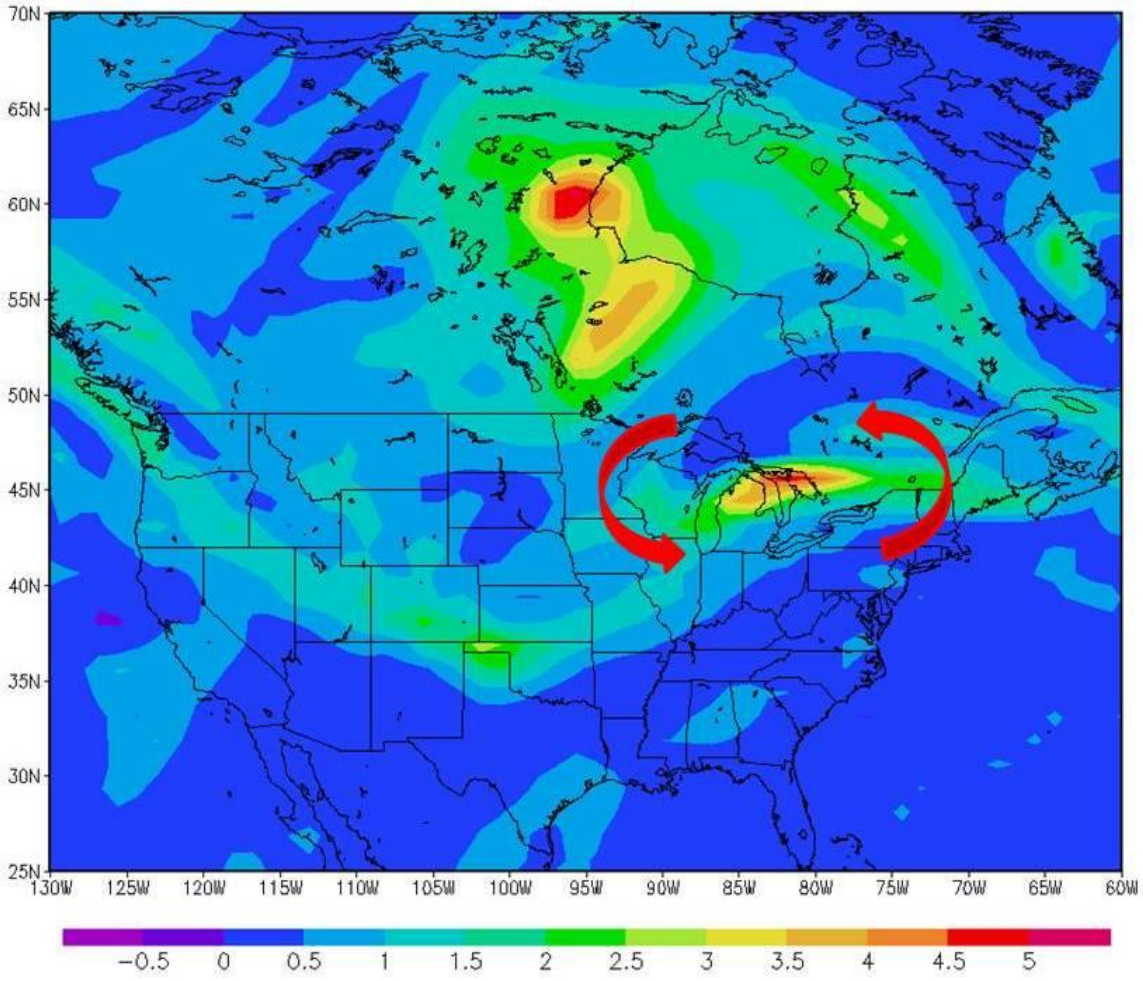

Figure 20 500 hPa MERRA Ertel Potential Vorticity field for 12z January 5. Color bar shading indicates values in potential vorticity units (PVU). Red arrows illustrate circulation induced by PV maximum.

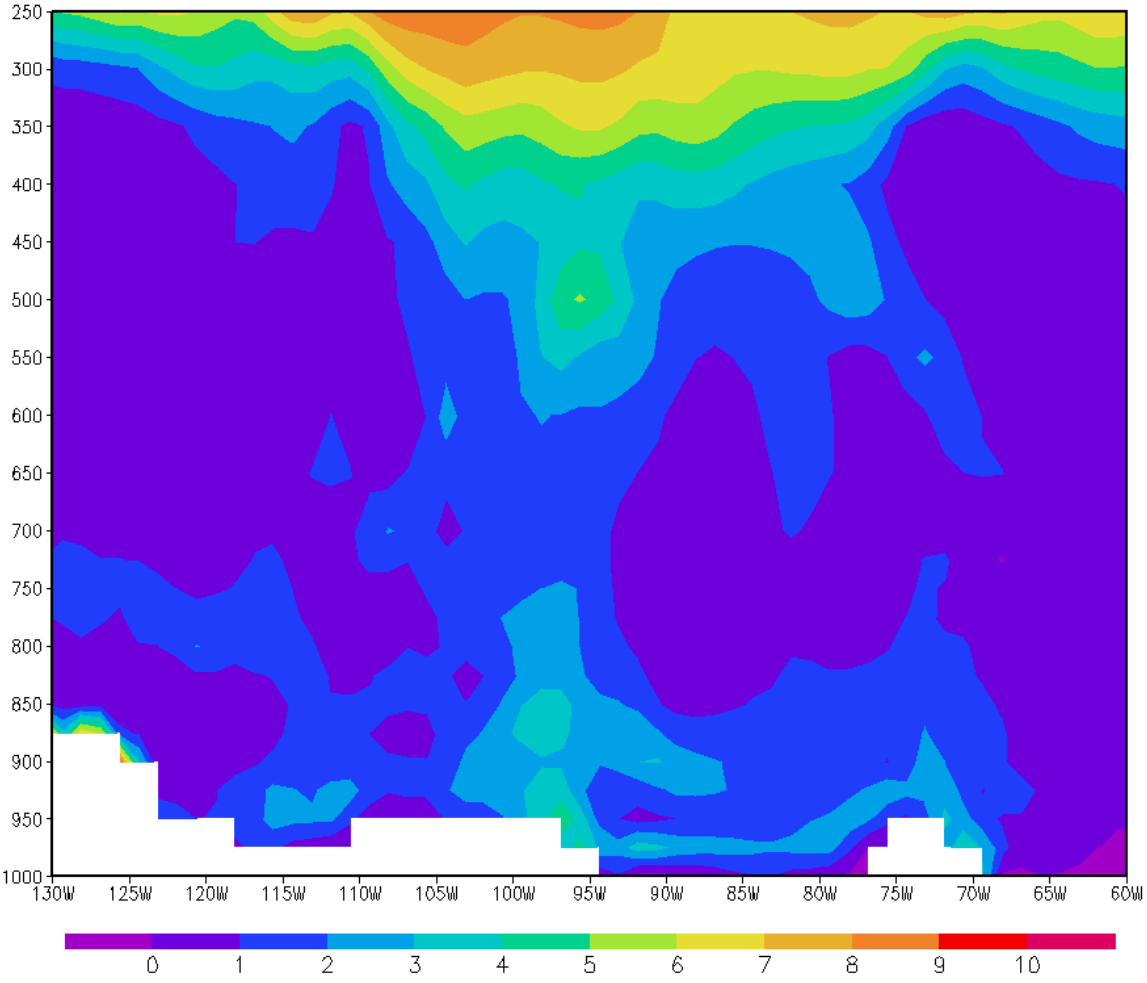

Figure 21 Vertical cross section (1000 hPa to 250 hPa) of Ertel Potential Vorticity averaged at 60N for 12z January 5. Color bar shading indicates values in PVU.

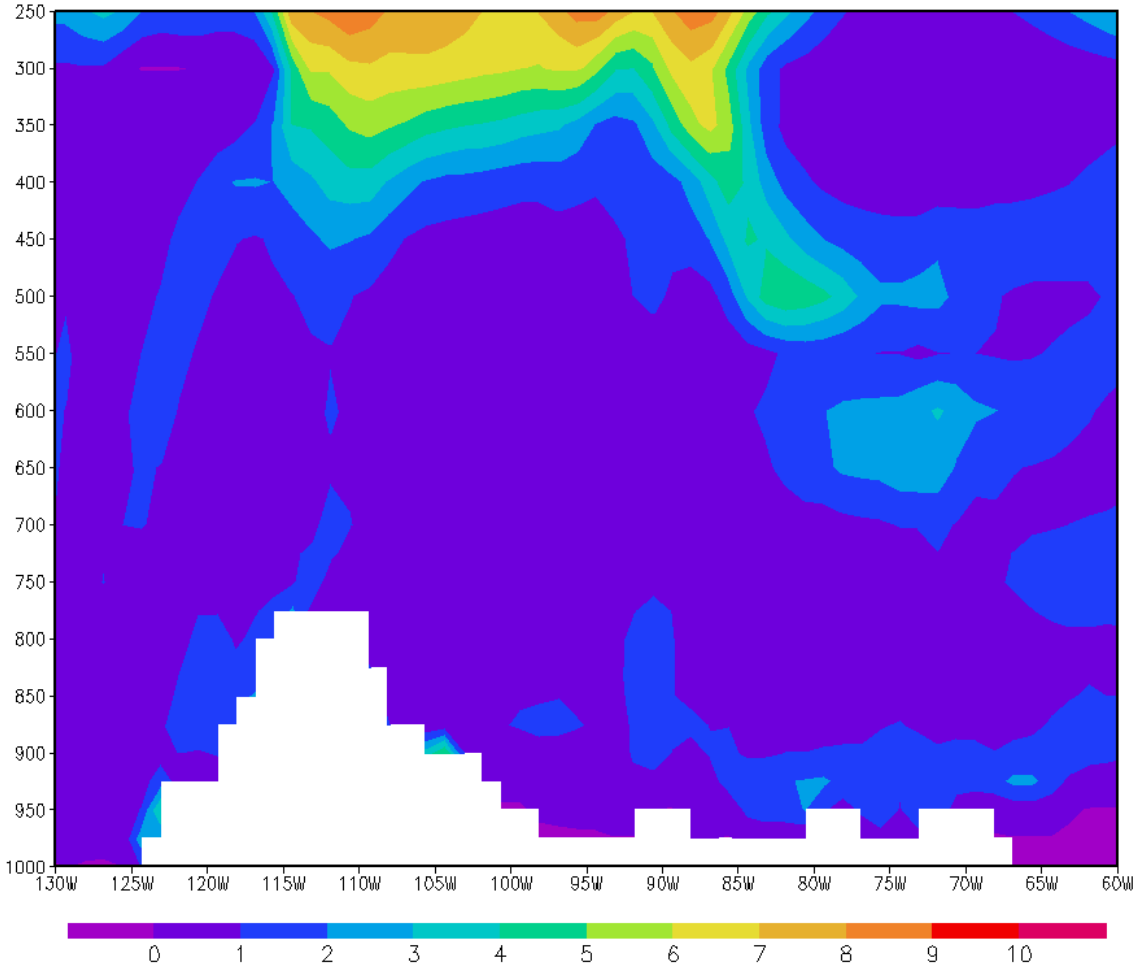

Figure 22 Vertical cross section (1000 hPa to 250 hPa) of Ertel Potential Vorticity averaged at 45N for 12z January 5. Color bar shading indicates values in PVU.

CHAPTER 4

CONCLUSIONS

Cold air outbreaks (CAOs) occurring during the boreal cool season have significant impacts upon the middle latitudes of the United States especially in heavily populated regions. The use of dynamical models can aid in predicting the outbreak of such extreme cold events and minimize the effects on society. A case study for the January 2004 CAO examined several reanalysis products through comparisons and assessment of reanalysis performance in relation to actual surface observations reported at various ASOS stations. Evaluation of reanalysis surface temperature performance displayed a prominent 18z cold bias in NCEP-NCAR over most of the continental United States with a 5-10 K bias over the southwest. As for specific humidity, all three reanalysis products overestimate the near surface specific humidity monthly mean at all hours with NCEP-NCAR performing exceptionally poor at 12z and 18z. NCEP-NCAR exhibits a qualitatively incorrect diurnal cycle for specific humidity with a peak at 12z, in contrast to a peak in observations at 00z. Although both MERRA and NARR overestimate the specific humidity diurnal cycle as well, NARR is better correlated to surface values observed at the selected ASOS stations.

The reanalyses and ASOS surface observations were also compared to evaluate the performance of the reanalysis products in capturing the frontal evolution and passage associated with the CAO. MERRA and NARR both out performed NCEP-NCAR in representing the detailed thermal and moisture structures associated with the leading cold front. MERRA performed the best overall for both the surface temperature and specific

humidity fields, but with NARR achieving equally high correlations for specific humidity. As a result, both MERRA and NARR provide useful observationally-based datasets for the study of CAO onset. Consequently, MERRA was utilized to study the dynamics behind the onset of the CAO through various lower and middle tropospheric variables in combination with surface temperature maps provided by NCEP HPC. The January 2004 event was marked by the buildup of a deep layer of cold air over central Canada that eventually migrated into the lower latitudes of the United States. The onset of the CAO was initiated by a cold front extending from a surface low pressure system located southeast of the Great Lakes. The dynamics of the synoptic system are linked to a tropopause fold event that occurred over the Great Lakes as was shown in the potential vorticity MERRA maps at 850 hPa and 500 hPa. The tropopause fold likely induced a broad cyclonic circulation that extended to the lower troposphere, helping to generate the southward excursion of the cold Canadian air.

REFERENCES

Cellitti M. P., Walsh J. E., Rauber R. M., Portis D. H., 2006: Extreme cold air outbreaks over the United States, the polar vortex, and the large-scale circulation. J. Geophys. Res., 111, D02114.

Danielsen, E. F., 1968: Stratospheric-tropospheric exchange based on radioactivity, ozone and potential vorticity. J. Atmos. Sci., 25, 502–518.

Downton, M. W., and K. A. Miller, 1993: The freeze risk to Florida citrus. Part II: Temperature variability and circulation patterns. J. Climate, 6, 364–372.

Kalnay, E., and Coauthors, 1996: The NCEP/NCAR 40-Year Reanalysis Project. Bull. Amer. Meteor. Soc., 77, 437–471.

Konrad, C. E., II, and S. J. Colucci, 1989: An examination of extreme cold air outbreaks over eastern North America. Mon. Weather Rev., 117, 2687–2700.

Mesinger, F., and Coauthors, 2006: North American Regional Analysis. Bull. Amer. Meteor. Soc., 87, 343–360.

Nogaj, M., P. Yiou, S. Parey, F. Malek, and P. Naveau, 2006: Amplitude and frequency of temperature extremes over the North Atlantic region. Geophys. Res. Lett., 33, L10801.

O'Neill M, Ebi K., 2009: Temperature extremes and health: impacts of climate variability and change in the United States. J. Occup. Environ. Med., 51, 13–25.

Osczevski, R., and M. Bluestein, 2005: The new wind chill equivalent temperature chart. Bull. Amer. Meteor. Soc., 86, 1453–1458.

Portis, D., M. Cellitti, W. L. Chapman, and J. E. Walsh, 2006: Low frequency variability and evolution of North American cold air outbreaks. Mon. Weather Rev., 134, 579-597.

Rao, T. N., J. Arvelius, and S. Kirkwood, 2008: Climatology of tropopause folds over a European Arctic station (Esrange). J. Geophys. Res., 113, D00B03.

Rogers, J. C., and R. V. Rohli, 1991: Florida citrus freezes and polar anticyclones in the Great Plains. J. Climate, 4, 1103–1113.

Rogers, J. C., and H. van Loon, 1979: The seesaw in winter temperatures between Greenland and northern Europe. Part II: Some oceanic and atmospheric effects in middle and high latitudes. Mon. Weather Rev., 107, 509– 519.

Suarez, M. J., and Coauthors, 2008: The GEOS-5 Data Assimilation System—Documentation of versions 5.0.1, 5.1.0, and 5.2.0. Vol. 27,NASATech. Memo.NASA/TM–2008–104606, 101 pp.

Thompson, D. W. J., and J. M. Wallace, 1998: The Arctic Oscillation signature in the wintertime geopotential height and temperature fields. Geophys. Res. Lett., 25, 1297–1300.

Thompson, D. W. J., and J. M. Wallace, 2001: Regional climate impacts of the Northern Hemisphere annular mode. Science, 293, 85– 88.

Vavrus, S., J. E. Walsh, W. L. Chapman, and D. Portis, 2006: The behaviour of extreme cold air outbreaks under greenhouse warming. Int. J. Climatol., 26, 1133–1147.

Walsh, J. E., A. S. Phillips, D. H. Portis, and W. L. Chapman, 2001: Extreme cold outbreaks in the United States and Europe. 1948 – 99, J. Climate, 14, 2642– 2658.

Wallace, J. M., and D. S. Gutzler, 1981: Teleconnections in the geopotential height field during the Northern Hemisphere winter. Mon. Weather Rev., 109, 784– 812.